Domino Ring Sampler (DRS) Performances in Dual-Readout Calorimetry

DREAM Collaboration[1]

N. Akchurin[a], F. Bedeschi[b], A. Cardini[c], R. Carosi[b], G. Ciapetti[d], R. Ferrari[e], S. Franchino[f], M. Fraternali[f], G. Gaudio[e], J. Hauptman[h], M. Incagli[b], F. Lacava[d], L. La Rotonda[h], S. Lee[g], M. Livan[f], E. Meoni[h,2], A. Negri[f], D. Pinci[d], A. Policicchio[h,3], S. Popescu[a], F. Scuri[b], A. Sill[a], G. Susinno[h], W. Vandelli[i], T. Venturelli[h], C. Voena[d], I. Volobouef[a] and R. Wigmans[a]

[a] *Texas Tech University, Lubbock (TX), USA*
[b] *I.N.F.N., Sezione di Pisa, Italy*
[c] *Dipartimento di Fisica, Università di Cagliari and I.N.F.N. Sezione di Cagliari, Italy*
[d] *Dipartimento di Fisica, Università di Roma "La Sapienza" and I.N.F.N. Sezione di Roma, Italy*
[e] *I.N.F.N., Sezione di Pavia, Italy*
[f] *Dipartimento di Fisica, Università di Pavia and I.N.F.N. Sezione di Pavia, Italy*
[g] *Iowa State University, Ames (IA), USA*
[h] *Dipartimento di Fisica, Università della Calabria and I.N.F.N. Sezione di Cosenza, Italy*
[i] *CERN, Genève, Switzerland*

Reference manuscript for the contribution to the 2010 IEEE Conference,
October 30 - November 6, 2010, Knoxville (TN), Usa

Abstract

First attempt to use last version (IV) of the Domino Ring Sampler (DRS) chip for time profile analysis of PMT signals produced in dual-readout calorimeters is described. Time characteristics of the signals sampled with a simple DAQ system based on the DRS-IV chip are compared with those of equal signals processed with a high performance digital oscilloscope. Separation between the fast Cherenkov and the slow scintillation components in the light signal produced by high energy electrons in a BGO crystal calorimeter is studied with data acquired with the two DAQ systems in identical beam and detector readout conditions. Studies of the pulse rise time and of the signal decay tail are presented in a time window of about 400 ns at sampling frequencies in the GS/sec region. Comparison of the preliminary results shows performances of the DRS based DAQ system equivalent to those of the digital oscilloscope for this application in dual-readout calorimetry.

[1]Corresponding author: Fabrizio Scuri, Istituto Nazionale di Fisica Nucleare, Sezione di Pisa, Italy - fabrizio.scuri@pi.infn.it

[2]Now at Department of Physics, University of Barcelona, Spain

[3]Now at Department of Physics, University of Washington, Seattle (WA), USA

1 Introduction

High sampling frequency and large bandwidth digitizers have been recently considered for many channel data acquisition systems in particle physics. The Domino Ring Sampler (DRS) chip, developed at P.S.I.[4], is a high performance device in the category of high frequency (up to 6 Gs/s) and large bandwidth (hundreds of MHz at -3 dB) samplers. Detailed descriptions of the principle and of the characteristics of the DRS chip can be found elsewhere [1]. Referring to figure 1, we just remind the principle of operation: the sampling frequency in the GHz range is generated with a series of inverters by a sampling signal freely propagating through these inverters in a circular fashion ("domino" principle). The analog input signal is stored in a switched capacitor array of 1024 cells. A trigger signal stops the running "domino wave", freezing the charge in the sampling capacitors. The individual cell contents are then read out by a shift register and digitized by a user select ADC, externally to the chip.

Earlier versions of the DRS chip are used to study the waveform of the liquid xenon calorimeter signal of the MEG experiment [2] for the $\mu^+ \to e^+\gamma$ decay search and to read out the MAGIC telescope experiment [3] to detect very high energy gamma-rays.

Due to its capability to perform time profile analysis over relatively large time windows ($\sim$ 500 ns at 2 Gs/sec, for instance), the DRS chip was first considered in the DREAM project [4] for dual-readout calorimetry to measure the fraction of kinetic energy carried by neutrons produced in hadronic showers; such a contribution is associated to a tail with characteristic time constant ($\sim$ 20 ns) in the scintillation signal produced in the DREAM fiber calorimeter [5]. Using a DAQ system derived from the MAGIC experiment one and based on version II of the DRS chip, DREAM measured the neutron fraction in hadronic showers [6]; comparable results were obtained with a DRS based DAQ system (38 channels) and with a much more expansive digital oscilloscope (4 channels).

Last version (IV) of the DRS chip implements relevant improvements with respect to the previous versions; in particular, intrinsic bandwidth for analog inputs is above 900 MHz at -3dB, maximum analog differential output non-linearity is 0.4 mV for differential analog inputs in the range [-0.5 V, +0.5 V], and thermal drifts of the offset is below 0.1 mV/°C at room temperature [7]. All these features, and mainly the expected overall large bandwidth ($>$ 400 MHz at -3dB) and the wide sampling time window, make DRS-IV a device suitable to process the signals generated by electromagnetic showers produced in dense doped crystals; the fast Cherenkov and the slower scintillation components in the produced light can be separated by time profile analysis of the readout pulse.

We present here a preliminary study of PMT signals produced by the readout system of a Bismuth Germanate ($Bi_4Ge_3O_{12}$ or BGO) crystal matrix, a homogeneous detector option for the electromagnetic section of the DREAM detector [8]. The signals produced by high energy electron beams crossing the BGO matrix are studied by comparing time profiles obtained with a DAQ system based on the DRS-IV chip and with a high performance digital oscilloscope in identical beam and readout conditions. The very simple DRS DAQ system used for this test is described in section 2; the experimental setup is described in section 3 and the results of the comparison are presented in section 4.

2 The DRS-IV evaluation board

Version IV is the latest upgrade of the DRS chip developed at P.S.I.; the simplified pin layout and the typical operation mode are shown in figure 2; a detailed description of the chip characteristics can be found in the documentation section of the DRS-IV web page [7].

The DRS-IV consists of an on-chip inverter chain generating a sampling frequency up to 6 GHz; the inverter system connecting adjacent cells is equivalent to a variable RC circuit formed

[4]Paul Scherrer Institut, Villigen, Switzerland

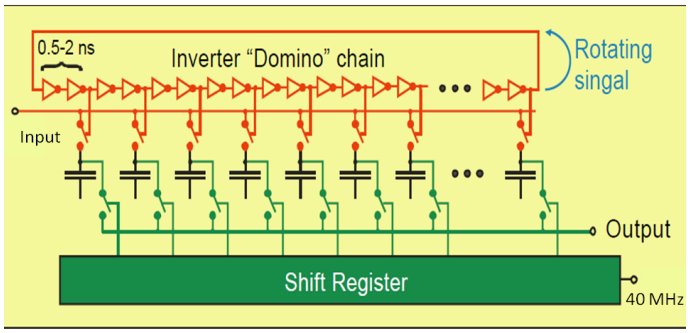

Figure 1: Simplified schematics of the DRS chip

by the parasitic input capacitance and by an equivalent voltage controlled resistor; sampling frequency is changed by varying the delay of propagation of the domino wave. This is controlled by the analog voltage applied on the DSPEED input. Stable operation at the desired sampling frequency is ensured by an internal PLL circuit driven by an external PLL loop filter.

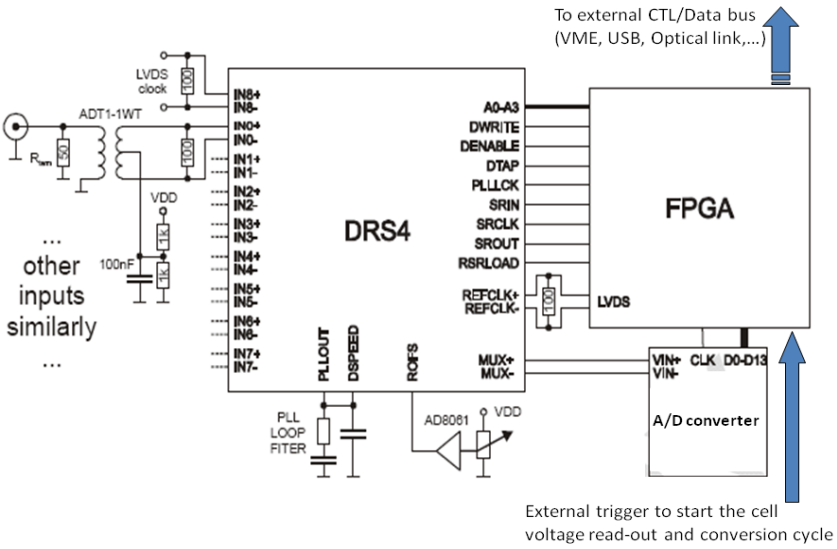

Figure 2: Typical operation mode of the DRS-IV chip

Nine differential input channels are present in the chip; typically, eight channels are allocated to the signals to be sampled, the ninth is left to sample the common trigger signal. An input driver block is required to convert single ended inputs into differential signals. Analog range for the input signal can be shifted into the chip linear region by setting an adjustable voltage value at the ROFS input, eventually using a DAC controlled by a FPGA. The individual cells of all nine channels are read out through multiplexers; they can be externally digitized in parallel or sequentially on MUX0+/MUX0-, as selected by the address lines A0-A3.

Address lines and digital signals used to configure the operation mode of the chip are con-

trolled by a FPGA. To determine the cell number where the sampling has been stopped by the trigger signal, a 10 bit stop shift register is used; it stores the cell number where the sampling has been stopped. Then, the full signal profile can be reconstructed starting from the stop cell by backwards scanning the full 1024 cell buffer, or, to reduce the dead time, by digitizing only a region of interest, defined by a selected number of contiguous cells starting from the stop one.

Commercial boards for DAQ systems based on DRS-IV are not yet available; therefore, to test the adequateness of DRS-IV in dual-readout calorimetry, we used some samples of a very simple board designed by P.S.I. developers and distributed for evaluating the chip performances [9]. The architecture of the evaluation board is shown in figure 3; four 50-Ohm terminated single ended analog inputs are received on SMA connectors in the front panel; transformers are used in the analog signal drivers to convert inputs into differential signals. Analog switches, following the transformers, allow the multiplexing of the DRS-IV inputs between the analog inputs and a reference voltage generated by an on-board 16-bit DAC for calibration purposes. The DRS-IV channels are sequentially converted by a 14-bit ADC at 33 MHz and read out by a FPGA which is used also to generate the control signals of the chip and to select the board operation mode. Data transfer from the FPGA memory buffer to the external proceed via an USB 2.0 connection, implemented with a micro controller, allowing for data transfer rates greater than 20 MB/sec.

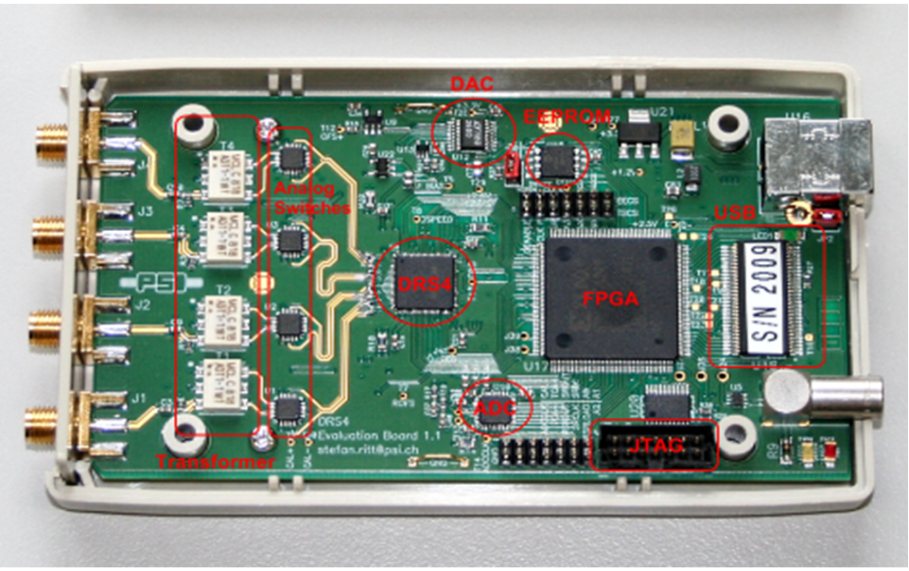

Figure 3: The DRS-IV evaluation board

The external trigger signal, 50-Ohm terminated TTL compatible, is received on a Lemo connector in the rear panel; an on-board discriminator with programmable level allows for self triggering on any of the input channels. An 1 MBit EEPROM is used to store the board serial number and calibration information. A JTAG adapter can be used to update the FPGA firmware.

3 Experimental setup

Time profiles of light signals produced by a BGO crystal marix were acquired in same beam and detector readout conditions with a digital oscilloscope and with a DAQ system including four DRS-IV evaluation boards. A sketch of the experimental setup is shown in figure 4. The

BGO calorimeter was placed in the H4 test beam line of the Super Proton Synchroton facility at CERN. Measurements described in this paper were performed with a 150 GeV electron beam.

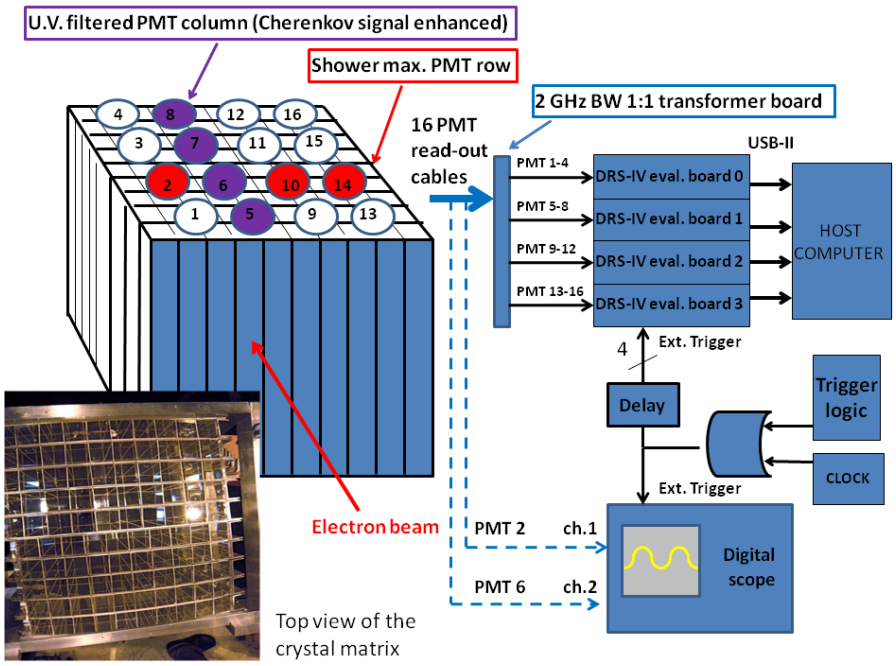

Figure 4: Simplified sketch of the experimental setup

We analyzed the light produced by the electrons crossing a 10 x 10 crystal matrix, corresponding to a section of the L3 electromagnetic calorimeter with projective geometry [10]; an array of 16 large area and large spectral window PMTs (Photonis XP3392B) was coupled to the matrix on the top of the detector, facing the larger end surface (3.2×3.2 cm^2) of the individual crystals, vertically oriented. The acceptance cone of each individual PMT covered many crystals and no particular attempt was done in the arrangement to avoid light mixing at the photo cathode from side columns and rows.

The light produced by electrons in the BGO crystals is dominated by the scintillation component which is characterized by a slow excitation and a very slow de-excitation process resulting in a very long decay time (about 300 ns at room temperature [11]) of the readout pulse. The small Cherenkov light component produced by the ultrarelativistic electrons can be measured by exploiting the spectral separation of the two light components [12]; the scintillation spectrum of BGO is centered around a wavelength of 480 nm. UV filters[5] were placed in front of the PMT cathodes used to readout the second column (figure 4) of the crystal matrix; the UV filters were transparent for light in the wavelength region from 250 to 400 nm. The residual scintillation component in the filtered signal was measured and subtracted using the method described in section 4.

The detector was mounted on a horizontal table which could be moved in the x-y plane orthogonal to the electron beam direction, allowing position scan in the vertical direction and along each crystal row of figure 4. Data presented in this paper were taken when the electron beam was crossing the detector at half hight in the vertical direction and in two different positions in the horizontal direction, corresponding to the axis of the PMTs in the first column (PMT 1 to 4, unfiltered) and of the PMTs in second column (PMT 5 to 8, UV filtered).

The 16 PMT signals were sent from the detector in the beam line to the counting room by 40 meter long low loss cables; signals were sampled and converted by a simple DAQ system made

[5]SCHOTT Filters UG-11

with four DRS-IV evaluation boards described in section 3. A common and delayed trigger signal was sent to each board by a trigger logic locked to the beam burst or by an external clock signal for pedestal events. High frequency transformers were used to invert the PMT signal polarity since, with the default firmware, the DRS-IV evaluation boards could not convert straight negative pulses from PMTs.The inverter transformer system acted as a high-pass filter and a distortion was introduced on the signals in input to the DRS. Such a distortion was off line corrected using the transfer function of the system; this was measured by injecting known waveforms in each transformer channel and by sampling and converting the inverted output with the same DAQ system used for electron beam data; in figure 5 is shown the transformer distortion (red curve) of a negative square pulse (5 ns rise time) generated with a waveform synthesizer; the black curve is the the same signal after correction with the measured transfer function. For the measurements presented here, the DRS-IV sampling frequency was set at 2 GS/sec and the full cell buffer was converted, allowing time profile analysis over a total time interval of 512 ns (1024 cells). The converted signals were stored on a host computer via USB 2.0 interfaces.

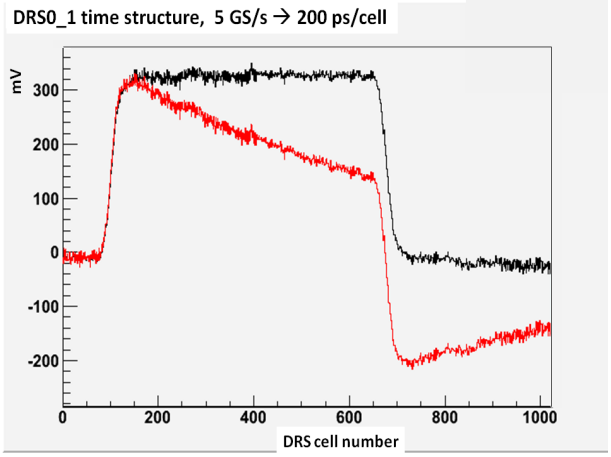

Figure 5: DRS time profile of a generated square pulse signal and distorted by the inverter transformers; red curve: raw signal; black curve: same signal, offline corrected with the measured transfer function of the transformer circuit.

Different runs in exactly equal beam conditions were taken by alternatively connecting cables from PMT-2 and PMT-6 to the DRS-IV DAQ system and to the input channels of a digital oscilloscope Tektronix TDS 7245B, 2.5 GHz analog bandwidth. The PMT signals were sampled with the oscilloscope every 0.8 ns over a total time interval of 424 ns (532 data points). The oscilloscope gain was chosen to reduce the overflow rate below 1%, optimizing the exploitation of the 8-bit dynamic range.

4 Comparison of time profile analysis with DRS-IV and digital oscilloscope

In the comparison of time profiles of signals sampled with the DRS system and with the digital oscilloscope our attention was focused on the shapes of the rise front and of the decay tail of the pulses. We analyzed signals produced by 150 GeV electrons in the section of the BGO crystal matrix readout by PMT_2 and PMT_6 of the second row of PMTs, corresponding to a detector depth approximatively between 5 and 10 cm where the shower maximum is reached.

We first checked the off line procedure to correct for signal distortions introduced by the transformers for DRS inputs; in figure 6 are shown two examples of single event time profile of DRS signals; black curves are the raw DRS outputs and red curves are the off line corrected signals.

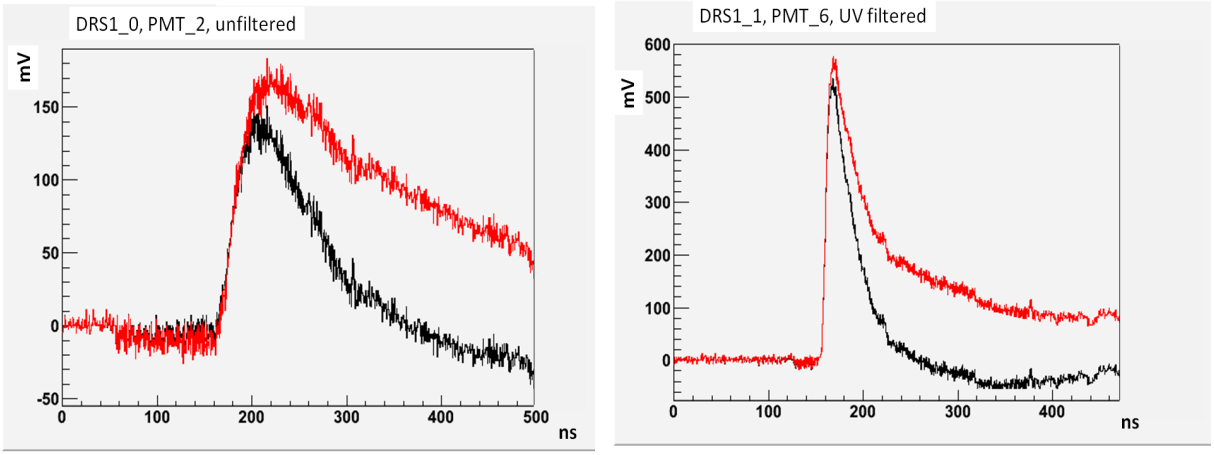

Figure 6: Single event time profiles; black curves: raw DRS sampled signals; red curves: DRS profiles after correction for transformer signal distortion.

To control possible biases introduced on DRS signals by the off line correction, we compared the BGO decay time of the unfiltered PMT_2 signal measured with DRS and digital oscilloscope; for a better visual comparison, the oscilloscope negative signal was off line inverted. Results of a single exponential fit to the tail of the sampled signals are shown in figure 7. Decay constant values of the fit function (parameter P2 in figure 7) are 265 ns for the DRS average time profile and 294 ns for digital oscilloscope; both values are close to the value 279 ns quoted in reference [11] for the slowest decay component of BGO at room temperature. The spread between the two values we measured is compatible with a temperature drift of a couple of centigrade degrees in the experimental area between different runs; the expected variation of the BGO slowest decay constant is of about -10 ns per °C [13].

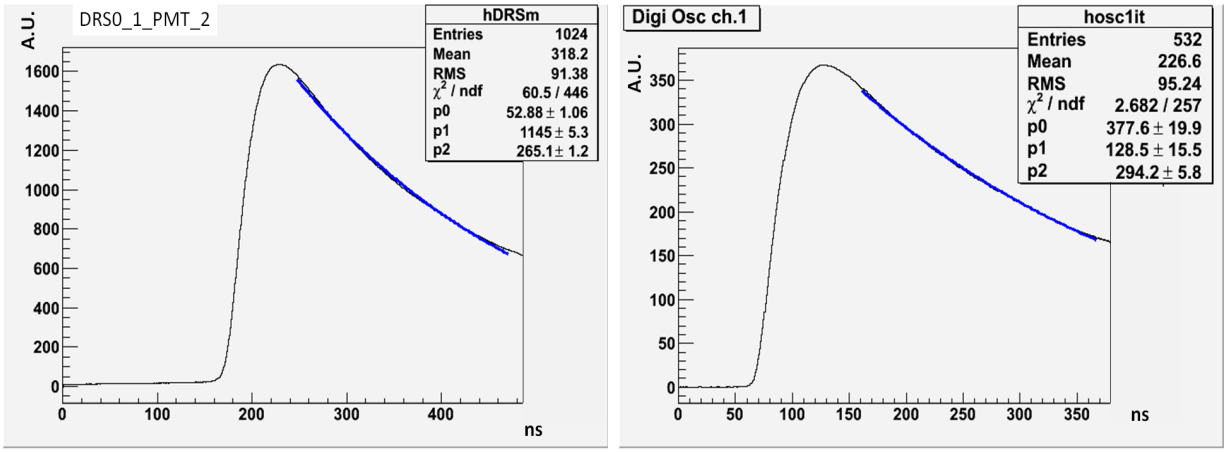

Figure 7: Average time profile (20,000 events) of the unfiltered PMT_2 signals; a single exponential function is fit to the signal tail.

In figure 8 is shown the rise front of DRS and digital oscilloscope signals; time profiles are the average on a single beam burst, about 1000 events.

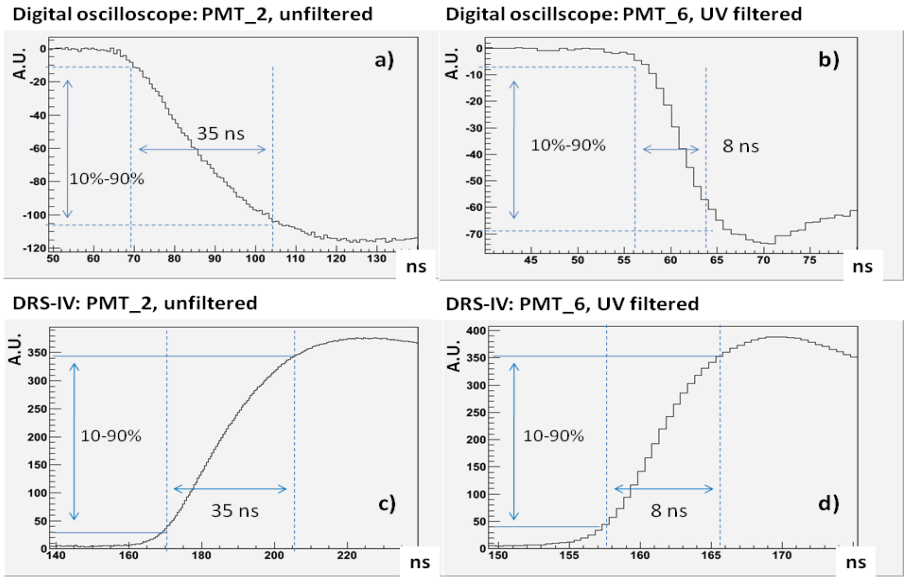

Figure 8: Comparison of pulse rise time signals of 150 GeV electrons at shower maximum in the BGO crystal matrix; a), b): digital scope; c), d): DRS-IV; figures a) and c) are relative to the not filtered PMT 2, figures b) and d) are relative to the UV filtered PMT 6.

Signals sampled with the digital oscilloscope (figures 8 a) and b)) and with the DRS-IV system (figures 8 c) and d)) show identical characteristics in the time window of the rise front; both scintillation signals (figures 8 a) and c)) from the not filtered PMT_2 have a 35 ns rise time which is determined by the slow excitation time of the BGO. Rise time of the UV filtered PMT 6 (figures 8 b) and d)) is about 8 ns; in this case the signal is formed by the prompt Cherenkov component superimposed to the residual scintillation component passing the UV filter (see figure 4) or coming from the side unfiltered crystals. Accurate analysis of the origin of such a relatively long rise time of the filtered signal is difficult and still in progress; the measured value is probably the result of the combined effects of PMT rise time (5 ns), of the slow residual scintillation component, and of the spread the optical path of the light produced in the Cherenkov cone around the beam axis, orthogonal to matrix crystal axes. What matters here is the fact that digital scope and DRS time profiles have exactly the same shape.

Information from the unfiltered PMT_2 signal and from the filtered PMT_6 signal was used in the procedure applied to extract the pure Cherenkov component. A template for the pure scintillation component was derived from the unfiltered average signal (figure 7) and used to model the residual scintillation component in the UV filtered signals. The black curves of figures 9a) (oscilloscope) and 9c) (DRS) are the average over 20,000 events of the genuine UV filtered signals; the red curves represent the residual scintillation component; they are obtained by folding the template of the scintillation signal to the full UV filtered signal (black curves) in a 200 ns wide gate starting 70 ns after the signal maximum; the blue curves represent the almost pure Cherenkov component and they obtained by subtracting the scintillation component (red curves) from the full signal (black curves). Baselines in figures 9a) and 9c) have the same temporal scale. In figures 9b) and 9d) is shown the fraction of the Cherenkov component (blue points) in the signal as a function of the integration gate width and relative to a reference gate 100 ns wide. The red triangle curves are the ratio of the scintillation component over the Cherenkov one as function of the gate width. All temporal gates used to measure those fractions are defined starting from the signal rise edge. Results summarized in figure 9 show again perfect

agreement between DRS-IV and digital oscilloscope analyses.

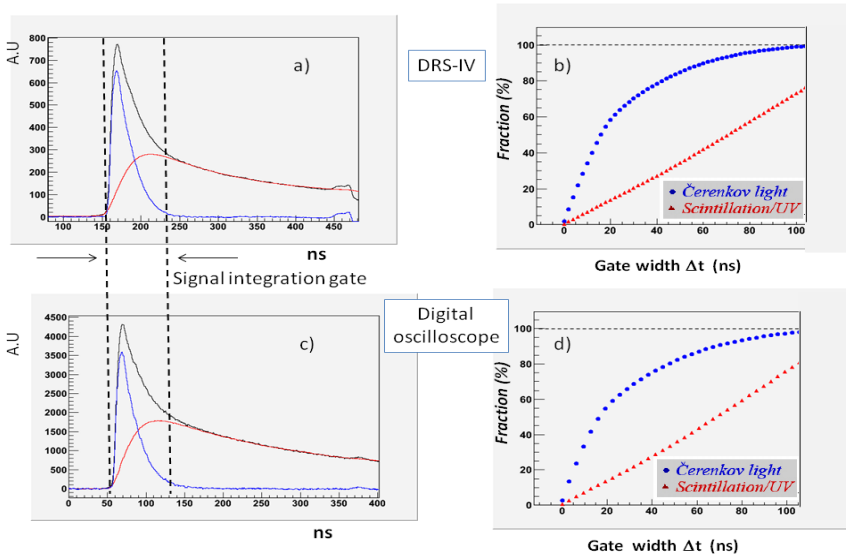

Figure 9: Comparison of time profiles of 150 GeV electron signals on BGO crystals; details in the text.

5 Conclusions

First attempt to use a DAQ system based on the DRS-IV chip in dual-readout calorimetry was satisfactory. Time profiles of PMT signals used to read out a BGO crystal matrix were produced with simple DAQ boards hosting the DRS-IV chip and with a high performance digital oscilloscope. Comparison of the results shows perfect agreement between the two systems. The simple tests described in the previous section spot the potentiality of DRS-IV based DAQ systems in high energy physics and, in particular, the possibility to separate scintillation and Cherenkov components of the light produced in dense doped crystal by high energy particles.

We presented here only a study on slow signals produced by a BGO crystal matrix; however, the DRS-IV characteristics are suitable for other specific applications in dual-readout calorimetry. For instance, the very high intrinsic bandwidth (900 GHz) can be exploited to reconstruct the short signals produced by small size fast crystals such as $PbWO_4$. On the other hand, the large sampling buffer (1024 cells) allows time profile analysis over large time windows as it is required, for instance, to detect the fraction of kinetic energy carried by neutrons generated in the shower development; this is related to the slower component in the tail of the signal generated by the sampling material in a detector with a high-Z absorber material.

We conclude by remarking that, once commercial VME cards will be available, the cost per channel of a DRS-IV based DAQ system is expected to be at least a factor 10 lower than in the case of equivalent commercial digital oscilloscopes, making realistic the projects to perform time profile analysis of individual signals from large channel number detectors.

Acknowledgements

We thank Dr. S. Ritt for his support on the use of the DRS-IV evaluation boards and the CERN for making particle beams of excellent quality. This study was carried out with the financial support of the Istituto Nazionale di Fisica Nucleare, Italy, and of the United States Department of Energy, under Contract DE-FG02-07ER41495.

References

[1] S. Ritt, Nucl. Instrum. Meth. **A 518** (2004) 470
R. Pegna et. al., Nucl. Instrum. Meth. **A 567** (2006) 218

[2] G. Signorelli, J.Phys. **G29** (2003) 2027.

[3] D.Ferenc, MAGIC Collaboration, Nucl.Instrum.Meth. **A 553** (2005) 274.

[4] R.Wigmans, Nucl. Instrum. Meth. **A 572** (2007) 215.

[5] N. Akchurin et al., Nucl. Instrum. Meth., **A 584** (2008) 273-284.

[6] M. Incagli, DREAM Collaboration, Nuclear Science Symposium Conference Record, 2008. NSS '08. IEEE, 19-25 Oct. 2008, pages 1673 - 1677.

[7] DRS-IV chip datasheet; http://drs.web.psi.ch/docs/DRS4_rev09.pdf.

[8] N. Akchurin et al., Nucl. Instrum. Meth., **A 609** (2009) 488-501.

[9] DRS4 evaluation board; http://drs.web.psi.ch/docs/manual_rev20.pdf.

[10] B. Adeva et al., Nucl. Instrum. Meth., **A 289** (1990) 35.

[11] M. Kobayashi et al., Nucl. Instrum. Meth., **A 372** (1996) 45-50.

[12] N. Akchurin et al., Nucl. Instrum. Meth., **A 598** (2009) 710-721.

[13] N. Tsuchida et al., Nucl. Instrum. Meth., **A 385** (1997) 290-298.